Nonlinear acceleration of dispersive effects in field line resonances

J. Y. Lu, R. Rankin, and R. Marchand
Department of Physics, University of Alberta, Edmonton, Alberta, Canada

V. T. Tikhonchuk
Institut de Physique Fondamentale, Université Bordeaux 1, France

Received 15 January 2003; revised 6 March 2003; accepted 17 April 2003; published 30 May 2003.

[1] Nonlinear dynamics of a dispersive field line resonance (FLR) is investigated in a dipolar magnetic geometry using a new finite element code TOPO. Time dependent dispersion and steepening of the perpendicular Alfvén velocity profile lead to the acceleration of dispersive effects and to localization of the FLR within an ionospheric density cavity. Consequently, shear Alfvén waves are trapped between turning points inside nonlinear density perturbations. This results in a complicated nonlinear FLR structure and an associated overlap of timescales for dispersion and nonlinearity. We show that nonlinear effects lead to fine scale structuring produced by the interplay of nonlinear and dispersive effects. We discuss the relevance of our results to observations of FLR's in the auroral zone. *INDEX TERMS:* 7827 Space Plasma Physics: Kinetic and MHD theory; 2704 Magnetospheric Physics: Auroral phenomena (2407); 2736 Magnetospheric Physics: Magnetosphere/ionosphere interactions; 2752 Magnetospheric Physics: MHD waves and instabilities. **Citation:** Lu, J. Y., R. Rankin, R. Marchand, and V. T. Tikhonchuk, Nonlinear acceleration of dispersive effects in field line resonances, *Geophys. Res. Lett.*, *30*(10), 1540, doi:10.1029/2003GL016929, 2003.

1. Introduction

[2] Sub-structure observed in low frequency auroral potential structures (discrete arcs on scales of 10–20 km) is often attributed to shear wave dispersion. Dispersion in shear Alfvén waves (SAWs) arises through electron inertia, electron thermal pressure, and ion gyro-radius effects. *Hasegawa* [1976] and *Goertz* [1984] have shown that electron inertia in SAWs can generate a parallel electric field capable of accelerating particles to hundreds of eV above the auroral ionosphere. Using a linear wave model, *Streltsov and Lotko* [1997] found that in a dipolar magnetic field, plasma parallel inhomogeneity can enhance SAW electric and magnetic fields, leading to dispersive field line resonances (FLRs) with ionospheric scale sizes of several kilometers.

[3] SAW dispersion and nonlinearity can strongly modify FLR dynamics. In particular, wave fields in FLRs can exert ponderomotive forces that drive density perturbations on auroral field lines. *Tikhonchuk et al.* [1995] used a simplified perturbative model to show that density perturbations take the form of a spectrum of slow magnetosonic waves which nonlinearly shift the frequency of the SAW. *Frycz et al.* [1998] derived reduced MHD equations for low frequency plasma and discussed the nonlinear interaction of dispersive FLRs and magnetosonic waves under an envelope (WKB) approximation in a Box model. *Rankin et al.* [1999] later extended the calculations of *Frycz et al.* [1998] into a dipolar model and showed that density cavity formation, and other observational features of auroral arcs, can be explained qualitatively in terms of ponderomotive forces and dispersive effects in FLRs.

[4] Nonlinear envelope models [*Frycz et al.*, 1998; *Rankin et al.*, 1999] are limited by assumptions of weak nonlinearity and wide separation of the Alfvénic, dispersive, and sonic time scales. Our studies show that on relaxing these constraints, strong wave-induced nonlinearity leads to confinement of wave energy inside latitudinally localized density perturbations. The wave fields are found to be finely structured due to a strong interplay between dispersive and nonlinear effects [*Samson et al.*, 1996]. We investigate these effects using a newly developed finite element simulation code [*Marchand and Simard*, 1997] which solves the full set of reduced MHD equations for dispersive FLRs in a dipolar geometry. Our non-perturbative treatment allows us to investigate the complete dynamics of growth and saturation of wave fields and density perturbations under realistic magnetospheric conditions. We demonstrate that a combination of dispersion and nonlinearity produces a rapid acceleration of dispersive effects in FLRs that are trapped inside ionospheric (equatorial) density cavities (bumps).

2. Reduced MHD Equations for Low Frequency Plasma Process

[5] The derivation of the reduced MHD equations describing the interaction of SAW and magnetosonic waves is based on the following assumptions [*Frycz et al.*, 1998]: (1) perturbations are characterized by a perpendicular scale length ($L_\perp$) that is much smaller than the parallel scale length ($L_\parallel$), i.e., $L_\perp/L_\parallel \ll 1$; (2) the characteristic time for the evolution of the wave is much longer than the ion gyro period, $1/\omega_{ci}t \ll 1$, where ω_{ci} is the ion gyro-frequency; (3) The electron inertia length λ_e and ion gyro radius ρ_i are small compared to the characteristic perpendicular scale: $(\lambda_e/L_\perp)^2 \sim (\rho_i/L_\perp)^2 \ll 1$; and (4) the plasma remains quasi-neutral. Following *Frycz et al.* [1998], we have rederived the reduced MHD Equations for low frequency plasma

$$\nabla\cdot\left[\frac{\rho\mu_0}{B_0^2}\left(1+\frac{3}{4}\rho_i^2\nabla_\perp^2\right)\frac{d}{dt}\nabla_\perp\phi\right]+\nabla\cdot\left(\mathbf{b}\nabla_\perp^2 A\right) = \nabla_\perp\cdot\left(\frac{\mu_0}{B_0}\mathbf{b}\times\nabla_\perp P\right), \quad (1)$$

0094-8276/03/2003GL016929

$$\frac{\partial A}{\partial t} + \mathbf{b}\cdot\nabla\phi = \lambda_e^2 \frac{\partial}{\partial t}\nabla_\perp^2 A + \frac{1}{en_e}\mathbf{b}\cdot\nabla P_e, \tag{2}$$

$$\rho\frac{dV_\parallel}{dt} = -\mathbf{b}\cdot\nabla P + \left(1+\frac{3}{4}\rho_i^2\nabla_\perp^2\right)\frac{\rho}{B_0^2}\nabla_\perp A\cdot\frac{d}{dt}\nabla_\perp\phi + \frac{1}{B_0}\mathbf{b}\cdot(\nabla_\perp A\times\nabla_\perp P), \tag{3}$$

$$\frac{1}{\rho}\frac{d\rho}{dt} = \frac{1}{B_0}\frac{\partial}{\partial t}\delta B_\parallel - \nabla\cdot\left(\mathbf{b}V_\parallel\right). \tag{4}$$

Here, A is the parallel component of the vector potential, ϕ is the scalar electric potential, ρ is the plasma density, B_0 is the unperturbed magnetic field, e is the elementary charge, P is the plasma pressure, P_e is the electron pressure, n_e is the electron number density, $\mathbf{b}$ is the unit vector along the magnetic field, $V_\parallel$ is the ion fluid velocity along the magnetic field, and $\delta B_\parallel$ is the compressional perturbation of the magnetic field. Equations (1) and (2) describe SAWs. Their coupling to density, pressure, and finite ion gyroradius effects are accounted for in (1), while (2) accounts for electron inertia and electron thermal pressure effects. Equations (3) and (4) describe magnetosonic waves. According to Ampere's law, $\delta B_\parallel$ is coupled to the plasma pressure through

$$\nabla_\perp\delta B_\parallel = -\frac{\mu_0}{B_0}\nabla_\perp P - \frac{\mu_0\rho}{B_0^2}\mathbf{b}\times\frac{d}{dt}\nabla_\perp\phi. \tag{5}$$

Note that our equations differ from that of *Frycz et al.* [1998] and *Rankin et al.* [1999] in that equation (2) is derived from the generalized Ohm's law without making an isothermal approximation. Here, the above set of equations is solved with a newly developed finite element code TOPO [*Marchand and Simard*, 1997] in an arbitrary two-dimensional curvilinear geometry assuming azimuthal symmetry.

3. Background Parameters

[6] We consider a two-species plasma with a constant density of hydrogen, $n_H = 1$ cm^{-3}, and an oxygen component with a density $n_O = 10^2$ cm^{-3} at the ionospheric ends which decreases exponentially with altitude over a scale length $h_O = 600$ km: $n_0(s) = n_H + n_O \exp[-(s_{max} - |s|)/h_O]$, where s is the coordinate along the magnetic field line, $s = 0$ at the equator, and the subscript "0" corresponds to the initial conditions of the related parameters. Along a given magnetic field line, the background electron and ion temperatures are initially chosen to satisfy the equilibrium condition of constant pressure, and the initial electron and ion temperature profiles are calculated from $\mathbf{B_0}\cdot\nabla(n_0 T_{e0,i0}) = 0$, using $T_{e0}^{eq} = 100$ eV and $T_{i0}^{eq} = 200$ eV at the equator. The time dependent plasma response is adiabatic with a constant ratio T_i/T_e along the field line.

[7] To excite a standing SAW in the magnetosphere, we impose a monochromatic driver by adding an electric potential ϕ to equation (1) of the form, $Q = Q_0 \sin(\omega_0 t)\exp(-[(x - x_0)^2 + z^2]/\Delta^2)$. Here, $x_0 = 7\ R_e$ and $\Delta = 0.5\ R_e$. The frequency ω_0 of the driver is resonant with the fundamental SAW mode at $L = 7$. We use a driver strength of $Q_0 = 2 \times 10^2$ V/s, corresponding to an effective driver $R = 2.5 \times 10^{-2}$ (see the definition of R, equation (7) of *Rankin et al.* [1999]). This choice was made to achieve a reasonable amplitude of the resonance fields, i.e., field aligned currents on the order of tens of $\mu A/m^2$ above the ionosphere [*Samson et al.*, 1996].

[8] Our choice of parameters corresponds to a SAW period of approximately 1.1 min and to a small negative dispersion parameter, $\delta = -5.04 \times 10^{-6} R_e^2$, where δ is related to the SAW frequency through the dispersion relation $\omega = \omega_0(1 + k_\perp^2\delta)$ (in the WKB approximation). For the definition of dispersive properties of a SAW standing along a magnetic field line, see equation (7) of *Rankin et al.* [1999]. The chosen SAW period is shorter than that found in typical observations. To lengthen the period, we have a choice of stretching the background field [*Rankin et al.*, 2000; *Lui and Cheng*, 2001] or invoking coupling of the SAWs to the slow acoustic mode [*Bhattacharjee et al.*, 1999]. This is beyond the scope here and a subsequent paper will discuss nonlinear and dispersive effects in a stretched topology.

4. Nonlinear Acceleration of Dispersive Effects

[9] During the initial temporal evolution of FLRs, nonlinear and dispersive effects are not important, and the imposed driver causes the SAW to narrow and grow linearly with time $\phi \propto A \propto t$. This is the linear phase mixing stage. The corresponding wave vector $k_\perp$ increases linearly with time, enhancing the wave dispersion that ultimately causes wave propagation in the perpendicular direction. The sense of propagation depends on the sign of the dispersion coefficient. Such a picture of the linear FLR evolution is shown in Figure 1a. For the parameters chosen, the dispersion coefficient is very small, and consequently perpendicular propagation of the SAW is not apparent.

[10] The ponderomotive force in equation (3) $\propto A\phi$ drives density perturbations which produce a nonlinear steepening of the perpendicular profile of the Alfvén velocity. Correspondingly, the frequency of SAW oscillations changes and this nonlinear frequency shift, $\delta\Omega$, increases in proportion to the magnitude of density perturbations $\delta\rho$ (which grow like t^2). The perpendicular derivative of the nonlinear SAW phase shift $\sim\delta\Omega t$ defines the perpendicular steepening scale $k_\perp \approx \delta\Omega t/l_\omega$, where l_ω is the characteristic scale length of the perpendicular variation of the SAW eigenfrequency. Evidently, due to nonlinear ponderomotive effects, $k_\perp$ increases with time much faster than it would due to linear phase mixing alone. Steepening must terminate at a level where dispersive effects come into play, at which point dispersive waves will be observed to propagate away from the resonant field line. This process is clearly seen in Figure 1b, where nonlinear phase mixing terminates at around 10 SAW periods. At that time, the dispersive term is of the same order of magnitude as the nonlinear term, $\delta\Omega = \omega_0 k_\perp^2\delta$, and this provides an estimate of the initial nonlinear phase mixing time, $t_{mix} = l_\omega/\sqrt{\omega_0\delta\Omega\delta}$. When nonlinearity dominates FLR evolution, dispersive scales appear after t_{mix}, and nonlinear dispersive waves propagate throughout the region where density perturbations are excited. In general, this scenario depends on the ambient field line parameters and on how strongly the resonant field line is driven. Associated characteristic amplitudes, timescales, and spatial scales can be estimated from the weakly

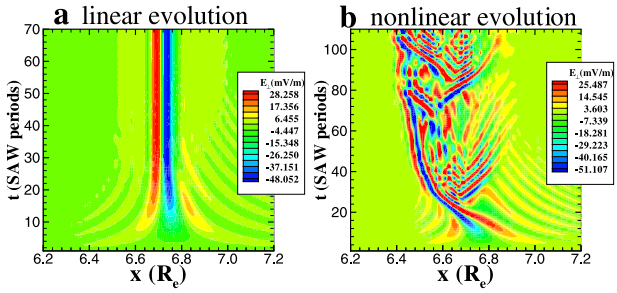

Figure 1. Dynamic evolution of electric field component perpendicular to the magnetic field $E_\perp$ at the equatorial plane in the (a) linear and (b) nonlinear cases.

nonlinear envelope approximation developed in *Rankin et al.* [1999].

[11] The example shown in Figure 1 shows the typical evolution of FLRs in the equatorial plane in the linear (Figure 1a) and nonlinear regime (Figure 1b), respectively. In comparing the striking differences in the time evolution of the electric field shown in panels a and b, we note that the linear case presents itself as a single standing wave structure in which dispersive effects are too small to make significant contributions to wave energy propagation. In the nonlinear case illustrated, nonlinearity and electron inertia attempt to move the resonance Earthward, while thermal effects work in the opposite direction. In Figure 1, inertial effects are larger than thermal effects. Thus, the resonance position moves Earthward, and a much broader and more complicated resonance structure is observed. According to the envelope approximation, the timescale t_{nl} for nonlinear ponderomotive effects is only a few SAW periods. This indicates a break-down of the envelope approximation in our earlier perturbative models, but points to strong nonlinear behavior at a modest SAW amplitude around $B_{nl} = 9$ nT.

[12] It is informative to compare the above estimates with the linear dispersive saturation time $t_d = 32$ SAW periods, and the dispersive saturation amplitude, $B_d = 225$ nT. We should also compare the nonlinear spatial scale $l_{nl} = 0.7\ R_e$ with the characteristic dispersive scale $l_d = 0.03\ R_e$. These estimates from *Rankin et al.* [1999] would seem to imply that for the chosen conditions, dispersion and nonlinearity

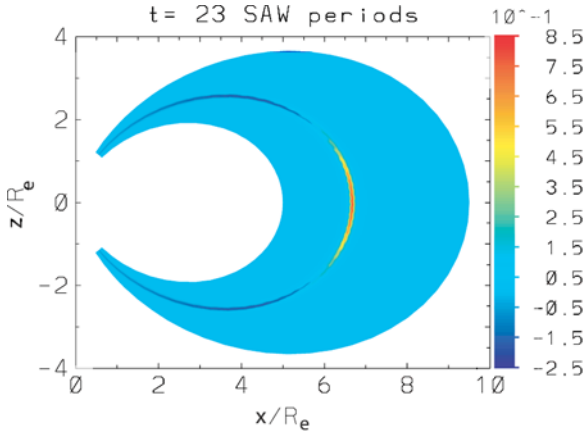

Figure 2. Relative density perturbation $\delta\rho/\rho_0$ of a nonlinear FLR at $t = 23$ SAW periods.

are spatially and temporally decoupled. However, they do not account for nonlinear modification of the spatial scale. The large density perturbation observed in Figure 2, which shows a 2D spatial distribution of the relative density perturbation along the field line at 23 SAW periods, changes the characteristic length scale of the radial variation of the SAW eigenfrequency. Our results show that at $t = 23$ SAW periods, l_ω decreases from 2.2 to 0.46 R_e at the equatorial plane, at $x = 6.7\ R_e$. The dispersive saturation time t_d is consequently reduced from 32 to around 9 SAW periods (i.e., comparable to the nonlinear timescale evident in Figure 2. and defined by $t_{\mathrm{mix}} = l_\omega/\sqrt{\omega_0\delta\Omega\delta}$), and the nonlinear spatial scale becomes 0.1 R_e, which is only three times larger than the dispersive spatial scales. Therefore, in this regime, there is actually a strong overlap between dispersive and nonlinear effects, and this is observed in Figure 1b and in Figures 2, 3 and 4.

[13] Figure 3 and Figure 4 show the radial dependence of the FLR at the equator, and at an altitude of 1.1 R_e, respectively. Note that according to Figure 2, the density perturbation occurs within a narrow region, creating turning points on either side of the resonance that trap the SAW inside the density perturbation. This slows down the SAW wave packet and after 30 periods it forms an almost stationary structure completely decoupled from the driver. This is clearly seen in Figures 1b and 3. At the same time, the driver continues to generate new SAWs which complicate the field structure and dynamics shown in Figures 3 and 4. A structure with a density bump at the equator (in

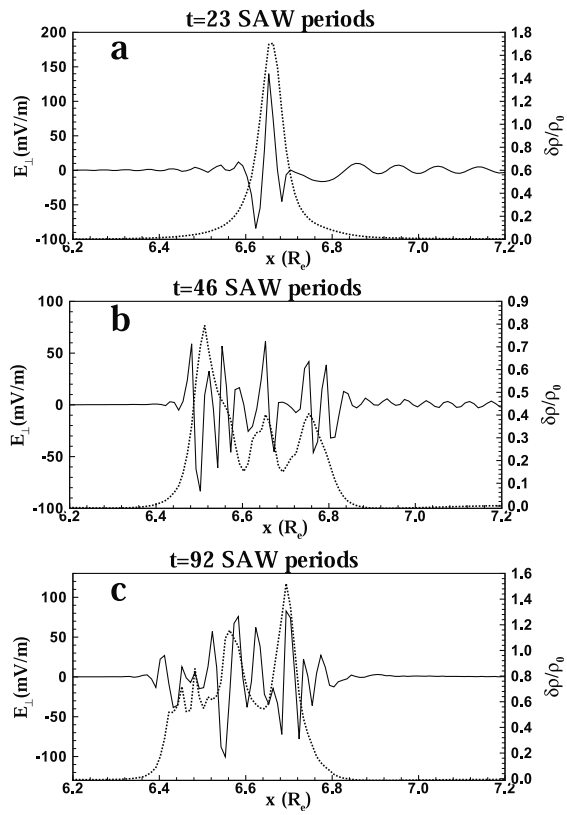

Figure 3. Radial dependence of perpendicular electric field (solid lines) and density perturbation (dotted lines) at the equatorial plane at t = (a) 23, (b) 46, and (c) 92 SAW periods.

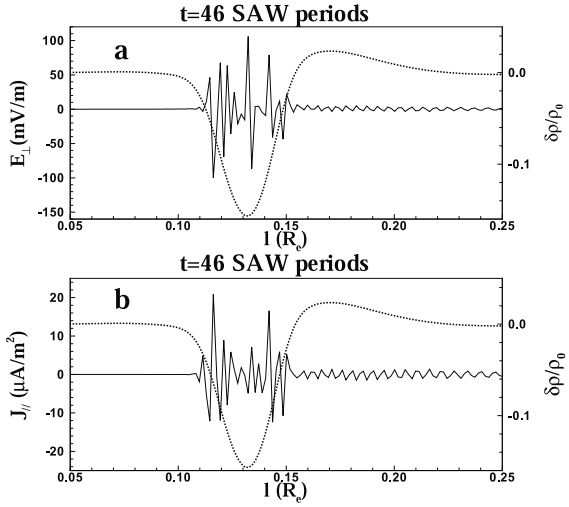

Figure 4. Spatial dependence of (a) perpendicular electric field and (b) parallel current across the magnetic field lines at an altitude 1.1 R_e for the time of 46 periods. The dotted line is the relative density perturbation. *l* corresponds to the distance in Earth radius from the inner boundary.

Figure 3) and a current carrying depletion above the ionosphere (Figure 4) can be unambiguously seen. The low altitude density depletions in our model may potentially explain those observed in satellite data. The localized substructuring of wave fields in our model also offers a possible explanation for certain features of long period auroral arcs [e.g., *Samson et al.*, 1991, 1996].

[14] Figure 2 demonstrates the field aligned density distribution. The parallel SAW structure corresponds to a magnetic field node in the equatorial plane and anti-nodes at the ionospheric ends. Correspondingly, the ponderomotive force pushes plasma towards the equator, creating a density bump in the FLR near the equatorial plane. This is the mechanism that decreases the FLR frequency, and the enhancement of the wave dispersion and eventual wave trapping. At the same time the ponderomotive force produces a strong density depletion near the ionospheric ends of the resonance field line.

5. Conclusion

[15] We have developed a new reduced MHD finite element code, TOPO, to investigate the nonlinear dynamics of dispersive field line resonances in a curvilinear geomagnetic field. We solve the full set of nonlinear reduced MHD equations self-consistently, without making use of the slowly varying amplitude (envelope) approximation. By relaxing the assumptions of the envelope model, we are able to study fine scale structuring of auroral arcs resulting from the interplay of enhanced nonlinear and dispersive effects.

[16] Our results show that FLRs are latitudinally localized within nonlinear density perturbations. Inside ionospheric (equatorial) density cavities (bumps), time dependent dispersion and steepening of the perpendicular Alfvén velocity profile lead to a rapid acceleration of nonlinear phase mixing and associated spacial structuring of FLR wave fields. We identify the appropriate timescales for dispersion and nonlinearity, and demonstrate that without nonlinearity, fine scale dispersive structuring may be difficult to achieve on auroral field lines that support FLR frequencies in the mHz range. The ionospheric density cavity may result in an enhancement of auroral electric fields [*Tikhonchuk and Rankin*, 2000], and can potentially explain density depletions that are a common feature of low altitude satellite data.

[17] In future work, we will address FLRs that are excited on stretched field lines characterized by specific solar wind conditions. This can potentially address FLRs with frequencies in the range of a number of observations [e.g., *Samson et al.*, 1991, 1996].

[18] **Acknowledgments.** This work was supported in part by CSA and NSERC and made use of MACI.

References

Bhattacharjee, A., C. A. Kletzing, Z. W. Ma, C. S. Ng, N. F. Otani, and X. Wang, Four-field model for dispersive field-line resonances: Effects of coupling between shear-Alfvén and slow modes, *Geophys. Res. Lett.*, *26*, 3281, 1999.

Frycz, P., R. Rankin, J. C. Samson, and V. T. Tikkonchuk, Nonlinear field line resonances: Dispersive effects, *Phys. Plasmas*, *5*, 3565, 1998.

Goertz, C. K., Kinetic Alfvén waves on auroral field lines, *Planet. Space Sci.*, *32*, 1387, 1984.

Hasegawa, A., Particle acceleration by MHD surface wave and formation of aurora, *J. Geophys. Res.*, *81*, 5083, 1976.

Lui, A. T. Y., and C. Z. Cheng, Resonance frequency of stretched magnetic field lines based on a self-consistent equilibrium magnetosphere model, *J. Geophys. Res.*, *106*(25), 27,793, 2001.

Marchand, R., and M. Simard, Finite element modelling of Tdev edge and divertor with $\mathbf{E} \times \mathbf{B}$ drifts, *Nucl. Fusion*, *37*, 1629, 1997.

Rankin, R., J. C. Samson, V. T. Tikhonchuk, and I. Voronkov, Auroral density fluctuations on dispersive field line resonances, *J. Geophys. Res.*, *104*, 4399, 1999.

Rankin, R., F. Fenrich, and V. T. Tikhonchuk, Shear Alfvén waves on stretched magnetic field lines near midnight in Earth's magnetosphere, *Geophys. Res. Lett.*, *27*, 3265, 2000.

Samson, J. C., T. J. Hughes, F. Creutzberg, D. D. Wallis, R. A. Greenwald, and J. M. Ruohoniemi, Observations of a detached, discrete arc in association with field line resonances, *J. Geophys. Res.*, *96*, 15,683, 1991.

Samson, J. C., L. L. Cogger, and Q. Pao, Observations of field line resonances, auroral arcs, and auroral vortex structures, *J. Geophys. Res.*, *101*, 17,373, 1996.

Streltsov, A. V., and W. Lotko, Dispersive, nonradiative field line resonances in a dipolar magnetic field geometry, *J. Geophys. Res.*, *102*, 27,121, 1997.

Tikhonchuk, V. T., and R. Rankin, Electron kinetic effects in standing shear Alfvén waves in the dipolar magnetosphere, *Phys. Plasmas*, *7*, 2630, 2000.

Tikhonchuk, V. T., R. Rankin, P. Frycz, and J. C. Samson, Nonlinear dynamics of standing shear Alfvén waves, *Phys. Plasmas*, *2*, 501, 1995.

J. Y. Lu, R. Marchand, and R. Rankin, Department of Physics, University of Alberta, 412 Avadh Bhatia Physics Laboratory, Edmonton, Alberta, Canada T6G 2J1. (jlu@space.ualberta.ca)

V. T. Tikhonchuk, Institut de Physique Fondamentale, Université Bordeaux 1, Le Haut Vigneau, B.P. 120, F-33175 Gradignan cedex, France. (tikhon@cenbg.in2p3.fr)